Filamentation of Femtosecond Laser Airy Beams in Water

Pavel Polynkin,* Miroslav Kolesik, and Jerome Moloney
College of Optical Sciences, The University of Arizona, Tucson, Arizona 85721, USA
(Received 2 March 2009; published 18 September 2009)

We report experiments on the propagation of intense, femtosecond, self-bending Airy laser beams in water. The supercontinuum radiation generated along the curved beam path is angularly resolved in the far field. Spectral maps of this radiation reveal the changing character of the laser-pulse evolution on propagation.

DOI: 10.1103/PhysRevLett.103.123902 PACS numbers: 42.65.Ky, 42.25.Bs, 42.65.Jx, 42.65.Re

Ultrafast laser filamentation is a rich, interdisciplinary branch of modern physics that deals with the propagation of ultraintense laser pulses in transparent dielectrics (see [1,2] for recent reviews). When an intense optical pulse propagates in a dielectric medium, the dynamic balance between various linear and nonlinear processes results in the formation of filaments, concentrations of electromagnetic energy that exhibit subdiffractive propagation over extended distances. High optical intensities inside filaments facilitate efficient nonlinear wavelength conversion, leading to the forward emission of broadband radiation. Analysis of the angularly-resolved spectral maps of this radiation (referred to as θ-λ or far-field spectra) yields insights into the pulse propagation dynamics [3–5].

Filamentation has been extensively studied both in solid and gaseous media, using various types of laser beams including Gaussian [6], flat-top [7], and Bessel beams [8,9]. In all of the above cases, the filaments were generated along straight lines, owing to the axial symmetry of the laser beams. The broadband forward emissions generated at different points along a straight filament overlap in the far field resulting in spectra that are difficult to interpret.

Recently, the generation of optical Airy beams has been reported [10]. These non axially-symmetric beams have two unusual properties: they are approximately diffraction free, and their main intensity features freely self-bend (or accelerate) on propagation in the absence of any refractive-index gradients in the medium.

Similar to Airy beams, so-called parabolic beams also resist diffraction and self-bend [11]. Generation of parabolic beams from Gaussian beams requires imposing complex modulation patterns on both the amplitude and phase profiles of the beam. Generating Airy beams is simpler as it requires phase modulation only.

It is instructive to compare accelerating beams with Bessel beams, which have been known of for quite some time [12]. In both cases the unusual properties of the beam result from the linear diffraction that continuously reshapes the transverse beam profile on propagation. In the case of a Bessel beam, the beam evolution results in the creation of an extended linear focus zone which is associated with ''diffraction-free'' propagation. In the case of an accelerating beam, the dominant intensity features in the beam cross section appear to shift sideways as the beam propagates. Even though the dominant features propagate along curved trajectories, the ''center of gravity'' of the beam pattern travels along a straight line.

An experimental study of filamentation with Airy beams in a gaseous medium (air) has been recently reported [13]. In a gas, the self-focusing collapse of the beam to a singularity is arrested by plasma defocusing. Results reported in [13] showed that the plasma channels generated through filamentation of Airy beams were bent and followed the curved trajectories of the laser beam.

Here we report experiments on filamentation of femtosecond Airy beams in a condensed medium (water). In this case, the group-velocity dispersion of the medium is the dominant mechanism that arrests the self-focusing collapse.

The experimental setup is shown schematically in Fig. 1. The femtosecond laser pulses are generated by a regeneratively amplified Ti:Sapphire laser system. The laser operates at a repetition rate of 10 Hz and generates 35 fs-long pulses with maximum pulse energy of 3.5 mJ, at 800 nm wavelength. The pulse energy is brought down to the μJ level by variable external attenuation. The laser beam has a Gaussian mode profile with 13 mm beam diameter at the $1/e^2$ intensity level.

The generation of Airy beams relies on the fact that the complex exponential in the form $\exp[i(\beta K)^3/3]$ and the

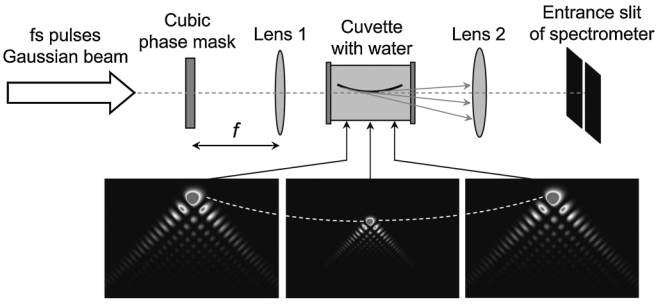

FIG. 1. Schematic of the experiment. The dominant lobe of the Airy beam pattern travels along a parabolic trajectory, as illustrated by the series of three intensity patterns in the bottom part of the figure.

Airy function $\mathrm{Ai}(x/x_0)$ form a Fourier-transform pair. (K, x are conjugate variables and β, x_0 are the appropriate scale factors.) Thus a two-dimensional (2D) Airy beam can be generated from a collimated Gaussian beam using a 2D cubic phase mask and a focusing lens [10].

The 2D phase mask used in our experiments is square, 2 cm $\times$ 2 cm in size. The total cubic phase *modulo* 2π varies between -68π and $+68\pi$ from one edge of the mask to the other, in both x and y dimensions. The Airy beam is formed in the vicinity of the focal plane of a lens with 25 cm focal length (Lens 1 in Fig. 1). The nonlinear self-focusing of the beam is studied in a 6.5 cm-long cuvette filled with water. The cuvette is positioned so that the focal plane of the lens is located in the middle of the cuvette.

The E-field amplitude of the two-dimensional, finite-energy Airy beam can be written as follows:

$$E(x, y) \propto \mathrm{Ai}(x/x_0)\mathrm{Ai}(y/x_0)\exp\left(a\frac{x+y}{x_0}\right), \qquad (1)$$

where (x, y) are the transverse coordinates, x_0 is a scale factor, and a is the so-called confinement parameter. For rough estimations of the beam parameters, we use approximate formulas for the linear propagation of quasi-cw Airy beams [10,13]. We find that the scale factor x_0 approximately equals 35 μm. d_0, the intensity FWHM of the dominant feature of the Airy beam pattern, can be estimated as $d_0 \approx 1.6x_0 \approx 55$ μm. The confinement parameter a is 0.032. The energy contained in the dominant intensity feature of the beam pattern is about 30% of the total pulse energy. The length of the diffraction-free propagation of the beam is estimated as 14 cm, which is over twice the length of the water cuvette. The beam acceleration defined as the ratio of the deviation of the beam trajectory from a straight line to the propagation distance squared, is estimated as 8×10^{-3} mm/cm^2. Over the entire propagation inside the water cuvette, the parabolic beam trajectory curves by $\sim$85 μm.

Under our experimental conditions, the forward emission by the filament becomes observable by the eye when the pulse energy reaches 9 μJ. This value of energy, assuming fully compressed 35 fs pulse, corresponds to the peak power of 260 MW, which is over 70 times higher than the self-focusing threshold for Gaussian beams in water. The high value of the self-focusing threshold for Airy beams is a consequence of their broad-angular content. The resistance of the broad-angular content beams to self-focusing collapse was previously observed for the case of filamentation of Bessel beams in water [8].

Immediately after the onset of filamentation, the emission pattern is dominated by isolated, approximately round spots. We observed one such spot for pulse energies between 9 μJ and 18 μJ, two spots in the range between 18 μJ and 24 μJ, and three spots in the range between 24 μJ and 35 μJ. Above 35 μJ, the emission pattern becomes irregular, likely due to the generation of multiple filaments within the dominant feature of the Airy beam.

In our setup, the orientation of the phase mask is such that the beam pattern accelerates vertically upwards. Accordingly, the generated filament is bent in the vertical plane, and the broadband forward emission in the far field is resolved along the vertical direction.

The following results were obtained at a fixed pulse energy of 20 μJ, at which the forward emission was dominated by two stable, partially overlapping round spots.

All images shown were taken using a commercial digital camera (Nikon, model D80). The images were obtained directly on the 12-bit CCD sensor of the camera, without using an objective lens. The wavelength sensitivity range of the camera was extended by removing the internal color filter [14]. The scatter of the primary laser light at 800 nm in the direct emission patterns was blocked by photographing these patterns through a color-glass filter (Shott Glass, filter BG39). This filter type is transparent in the wavelength range from 350 nm to 700 nm, and has a very high optical density for wavelengths above 750 nm. Only single-shot images were taken. The zero angle in the images was identified by a visible cw laser beam sent along the optical axis of the setup. The diameter of this reference beam was much smaller than the size of the features on the phase mask. The reference beam experienced negligible phase modulation and propagated along a straight line.

A photograph of the full direct emission pattern is shown in Fig. 2(a). The angle scale in this image was calculated from the size of the CCD sensor and the distance from the water cell to the camera. From the rate of the beam deflection estimated above, the origin of the bottom spot in the emission pattern can be traced to the very entrance of the water cell. Thus the beam undergoes filamentation immediately after entering the cell. This is consistent with the estimated value of $\sim$0.5 mm for the distance to the self-focusing collapse point [15]. In the estimation, we used the fact that the dominant feature of the Airy beam in our case carries about 30% of the total beam energy and assumed that this feature undergoes a rapid collapse on its own, without being affected by the rest of the beam pattern.

The exact location of the upper spot in the emission pattern of Fig. 2(a) experienced vertical fluctuations from one laser shot to another. Accounting for these fluctuations, the origin of this spot can be traced to somewhere between 4 cm and 6 cm from the entrance to the cuvette.

By placing a 150 μm-diameter aperture inside the water cell at a distance of 15 mm from the cell entrance and adjusting the position of the aperture in the transverse plane, the upper spot can be removed from the emission pattern, while minimally affecting the lower spot, as shown in Fig. 2(b). The properly positioned aperture only passes the forward emission generated in the beginning section of the filament. At the same time, the entire Airy beam pattern is blocked at the plane of the aperture, and there is no filament formed after that plane. An alternative way of achieving longitudinal resolution in studies of forward emission by filaments relies on using a syringelike water cell with variable length [16].

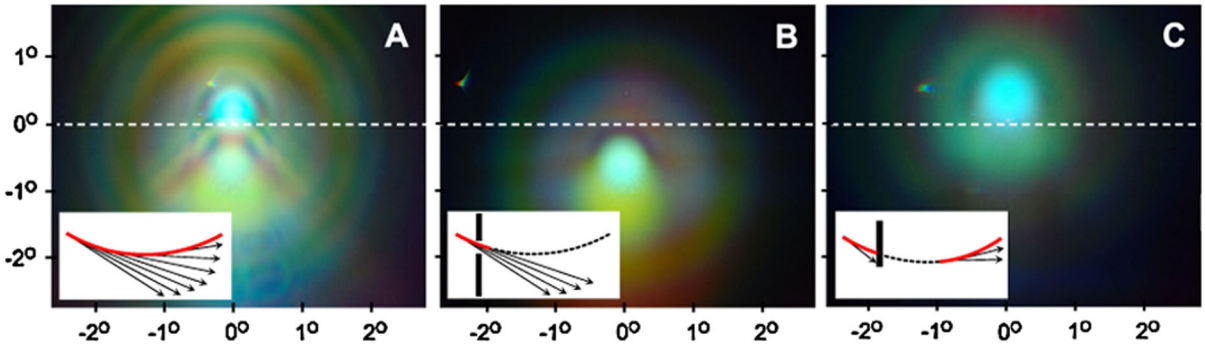

FIG. 2 (color online). Photographs of the forward emission patterns by bent filament. The insets illustrate how the emission originating from different sections of the filament is isolated from the rest of the emission. (a) Complete emission pattern. (b) Emission pattern from the beginning section of the filament. (c) Emission pattern from the end section of the filament.

By placing a properly positioned edge obstruction into the beam at the same distance of 15 mm from the entrance to the cell, the emission originating from the beginning section of the filament can be removed from the pattern, as shown in Fig. 2(c). The edge obstruction completely blocks the emission resulting from the first self-focusing collapse event that occurs immediately after the pulse enters the water cell. At the same time, the edge also blocks the tip of the Airy beams pattern, while the rest of the pattern passes freely. Because of the self-healing properties of Airy beams [17], the beam pattern reconstructs itself after propagating a finite distance from the plane of the obstruction, and the end section of the filament is restored.

The above approach relies on the self-bending property of the Airy beam. The application of this technique is limited by the finite propagation distance that is necessary for the beam to restore its dominant intensity feature after the feature is blocked by the edge obstruction. Thus the radiation emanating from the middle section of the filament is inadvertently affected by the insertion of the obstruction. In our case, the emission along the filament consists of two separated spots; thus, the emission originating from the end section of the filament, which corresponds to the upper spot in the emission pattern, can be isolated cleanly. The refinement of this approach is, in principle, possible, by using a combination of edge and aperture obstructions.

As we mentioned earlier, θ-λ spectra of the forward emission convey information about pulse dynamics inside the core of the filament. To study this type of spectra in the case of filamentation of Airy beams in water, we apply the imaging spectrometer technique [3]. The resulting spectral maps of the forward emission are shown in Figs. 3(a)–3(c). These images correspond to the direct emission patterns of Figs. 2(a)–2(c), respectively. No color filtering was used in photographing the spectra. Three narrow-line laser sources, with wavelengths of 800 nm, 633 nm and 532 nm were used to calibrate the spectrometer setup.

Figure 3(a) shows the complete emission spectrum. This pattern consists of the stacked-up spectra originating from different segments of the filament and shows a substantial degree of overlap between the individual spectra.

As in the case of direct emission patterns, the contributions from the emission originating from the beginning and the end sections of the filament can be separated from the complete pattern by inserting obstructions into the beam path. In this technique, the contribution from the middle section of the filament is, in general, lost. Nevertheless, the

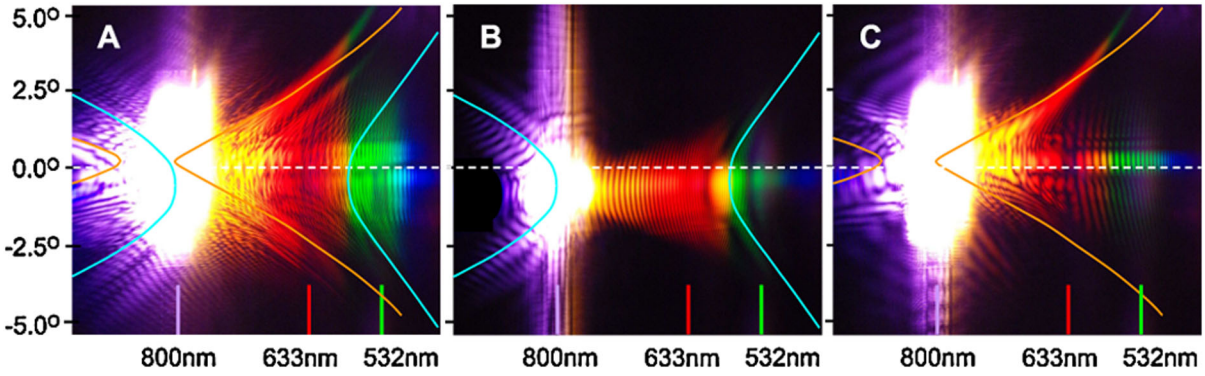

FIG. 3 (color online). θ-λ spectral maps of the forward supercontinuum emission. (a) Complete emission pattern. (b) Emission from the beginning section of the filament. (c) Emission from the end section of the filament. In figures (b) and (c), the best-fit curves based on the effective three-wave mixing approach are shown with light blue and orange solid lines. Same best-fit curves are also shown in the complete pattern (a).

comparison between the complete pattern of Fig. 3(a) with the patterns shown in Figs. 3(b) and 3(c) shows that the dominant features in these patterns can indeed be isolated. These so-called X-wave signatures (long, diagonal arms extending at the either side of the fundamental wavelength) are characteristic of pulse-splitting events [4].

Resolution of spatial and spectral features downstream along the propagation path remains an open theoretical problem due to the lack of axial symmetry of the Airy beam and the strong nonlinear dispersive (k-ω) coupling. Consequently the problem is three dimensional and is complicated further by the fact that energy feeding in from the periphery of the beam pattern strongly modifies the nonlinear core that acts as the scattering potential that generates spectral components. Direct numerical simulation is beyond our computational capabilities.

Instead of simulating the spectra directly, we use the fitting procedure based on the effective three-wave mixing (ETWM) picture [5]. In the ETWM approach, the supercontinuum generation is interpreted as a result of a linear scattering of the incident laser pulse on a ''material wave,'' which closely follows the spatially localized, temporally split waveform inside the core of the filament. The filling of the θ-λ spectral map is governed by the phase-matching conditions for this scattering process. By fitting different branches in the spectra with the phase-matching conditions, one can, in principle, deduce the effective group velocities of the subpulses comprising the temporal waveform in the core of the filament.

The ETWM-based fitting procedure has been successfully used in various cases of filamentation with weakly focused Gaussian beams, but its applicability to more complex beams such as Airy beams has not been verified. As we found, the ETWM-based procedure works quite well for the emission from the beginning section of the filament. In Fig. 3(b), the best fit to the green arc around 500 nm and the corresponding X features on the longer wavelength side are shown with the solid light blue lines. From the fitting parameters we deduce that these spectral features are likely to be produced by a trailing subpulse inside the filament core. This subpulse travels with the effective group velocity of $(1 - 0.0035)v_g$, where v_g is the linear group velocity in the medium.

If applied to the spectrum from the end section of the filament, the ETWM picture fails to produce a reasonable fit. In Fig. 3(c), we show an attempt to fit the extended diagonal red arm in the spectral pattern. The agreement between the best fit (corresponding to a leading subpulse with the effective group velocity of $(1 + 0.0005)v_g$) and the data is only qualitative. The only conclusion that can be drawn based on the data is that the diagonal spectral feature is likely to be produced by a leading subpulse inside the filament core, but the effective velocity of this subpulse cannot be found because of the poor fit quality.

The reasons why the ETWM picture works well for the beginning section of the filament but does not work for the end section are still under investigation. Qualitatively, we argue that in the beginning section, the self-focusing collapse of the compressed 35 fs pulse occurs rapidly, so that the dominant intensity feature of the beam collapses on its own, without any influence from the remaining beam pattern. The collapse occurs as if the dominant feature were an isolated, approximately round focused beam and the ETWM picture that is applicable for filamentation of smooth round beams is adequate.

In the end section of the filament, the pulse propagates in the water for about 5 cm and has broadened to ~100 fs by the water group-velocity dispersion. The second collapse event occurs more gradually, and is affected by the bending of the beam. Furthermore, the secondary features of the Airy beam pattern are likely to start self-focusing on their own. The ''material wave'' is no longer localized inside of the dominant beam feature, but includes contributions from the secondary features. The apparent asymmetry of the spectral pattern in Fig. 3(c) with respect to the angle inversion is an indication that the scattering potential in this case is indeed not symmetric.

This work was supported by The United States Air Force Office of Scientific Research under programs FA9550-07-1-0010 and FA9550-07-1-0256. The authors thank G. Siviloglou and D. Christodoulides of the University of Central Florida and D. Faccio and P. Di Trapani of the University of Como, Italy, for numerous fruitful discussions. We also acknowledge contribution of D. Hansen and T. Milster of the University of Arizona who fabricated cubic phase masks used in the experiments.

*ppolynkin@optics.arizona.edu

[1] A. Couairon and A. Mysyrowicz, Phys. Rep. **441**, 47 (2007).
[2] L. Berge, S. Skupin, R. Nuter, J. Kasparian, and J.-P. Wolf, Rep. Prog. Phys. **70**, 1633 (2007).
[3] D. Faccio *et al.*, J. Opt. Soc. Am. B **22**, 862 (2005).
[4] M. Kolesik, E. Wright, and J. Moloney, Opt. Express **13**, 10 729 (2005).
[5] M. Kolesik and J. Moloney, Opt. Express **16**, 2971 (2008).
[6] A. Braun *et al.*, Opt. Lett. **20**, 73 (1995).
[7] S. Tzortzakis *et al.*, Opt. Lett. **25**, 1270 (2000).
[8] A. Dubietis *et al.*, Opt. Express **15**, 4168 (2007).
[9] P. Polynkin *et al.*, Opt. Express **16**, 15 733 (2008).
[10] G. Siviloglou, J. Broky, A. Dogariu, and D. Christodoulides, Phys. Rev. Lett. **99**, 213901 (2007).
[11] J. Davis, M. Mitry, M. Bandres, and D. Cottrell, Opt. Express **16**, 12 866 (2008).
[12] J. Durnin, J. Miceli, and J. Eberly, Phys. Rev. Lett. **58**, 1499 (1987).
[13] P. Polynkin, M. Kolesik, J. Moloney, G. Siviloglou, and D. Christodoulides, Science **324**, 229 (2009).
[14] D. Faccio (private communication).
[15] J. Marburger, Prog. Quantum Electron. **4**, 35 (1975).
[16] A. Dubietis *et al.*, Appl. Phys. B **84**, 439 (2006).
[17] J. Broky, G. Siviloglou, A. Dogariu, and D. Christodoulides, Opt. Express **16**, 12 880 (2008).